Conf-911179--4

DISCLAIMER

WSRC-MS--90-317

DE92 010097

CORROSION TESTING OF TYPE 304L STAINLESS STEEL FOR WASTE TANK APPLICATIONS (U)

by

B. J. Wiersma, et al

Westinghouse Savannah River Company
Savannah River Site
Aiken, South Carolina 29808

A paper proposed for presentation at the
Life Prediction of Corrodible Structures Meeting
Kauai, Hawaii
November 5-8, 1991

and for publication in the proceedings

This paper was prepared in connection with work done under Contract No. DE-AC09-89SR18035 with the U.S. Department of Energy. By acceptance of this paper, the publisher and/or recipient acknowledges the U.S. Government's right to retain a nonexclusive, royalty-free license in and to any copyright covering this paper, along with the right to reproduce and to authorize others to reproduce all or part of the copyrighted paper.

Corrosion Testing of Type 304L Stainless Steel for Waste Tank Applications

Bruce J. Wiersma
Westinghouse Savannah River Company
Savannah River Laboratory
Box 616
Aiken, SC 29808

John I. Mickalonis
Westinghouse Savannah River Company
Savannah River Laboratory
Box 616
Aiken, SC 29808

Abstract

AISI Type 304L stainless steel will be the material of construction for hazardous waste storage tanks. The corrosion behavior of 304L was characterized in simulated waste solutions using potentiodynamic polarization, electrochemical impedance spectroscopy and long term immersion tests. The results were correlated to assess the use of corrosion characteristics determined by electrochemical techniques for predicting long term corrosion behavior. The corrosion behaviors of Type A537 carbon steel and Incoloy 825 were also evaluated. A good correlation was found between the results from the electrochemical techniques and the immersion tests.

Key terms: potentiodynamic polarization, impedance spectroscopy, immersion tests, stainless steels, localized corrosion

Introduction

Minimization and disposal of radioactive waste is a major priority at the Savannah River Site. A variety of wastes, generally in the form of inorganic salt slurries, are generated by processes such as chemical separation of reactor products, cleaning of reactor targets and regeneration of moderator deionizing resins. Wastes from the reactor products are decontaminated and routed to either a facility which encapsulates the waste in borosilicate glass[1] or to a facility which converts the waste in to a cement-like material known as

saltstone. The cleaning and regeneration solutions are also decontaminated and sent to an effluent treatment facility.

Prior to these disposal processes, the salt slurries are washed to remove the insoluble salts. The supernate from the washed slurry is routed to holding tanks and stored there until it is recycled back into the process as a wash stream. The available facilities for storage of the wash solutions are single-walled carbon steel tanks. Since the wastes are generated from several different sources, these tanks must be corrosion resistant over a wide range of solution compositions.

Laboratory tests and in-service observations revealed that carbon steel was not resistant to uninhibited waste solutions. Coupon tests performed in simulated waste indicated that the carbon steel tanks were susceptible to localized corrosion in a wetted film region above the water line[2]. This attack was induced by nitrate and resulted from the depletion of the hydroxide inhibitor which occurred due to the absorption of CO_2 in the wetted film. In-service inspection of carbon steel tanks which stored uninhibited waste solutions revealed that the non-immersed area of the tank wall was covered with broad shallow pits, while the immersed area did not corrode. Sodium nitrite was identified as an effective inhibitor for nitrate corrosion of carbon steel[3]. Since the concentration of the anions in the wash water may vary from their average value by ± 30 %, excess nitrite maybe required to inhibit corrosion. Increased inhibitor requirements increase cost and may adversely affect the encapsulation of the waste in the glass. A proposal to design and construct new tanks was made to minimize the need for increased inhibitor and to reduce surveillance frequency. The candidate material of construction for these tanks was AISI Type 304L stainless steel (304L). 304L may be susceptible to localized corrosion in the wastes due to the presence of chlorides and fluorides[4].

Laboratory tests were conducted to confirm the suitability of 304L for long-term waste storage. These tests included short-term cyclic polarization and four-month coupon immersion tests. Electrochemical impedance spectroscopy (EIS) was used to monitor the corrosion process on a few samples during the coupon tests. The test materials were 304L, A537 carbon steel (A537), and Incoloy 825 (I825). A537 and I825 are materials which are less and more corrosion resistant than 304L, respectively.

Experimental Procedure

The Princeton Applied Research (PAR) Model 351 Corrosion Measurement System was used to control a Model 273A Potentiostat/Galvanostat to obtain the cyclic polarization scans. A PAR electrochemical cell held the specimen in an unstirred and aerated solution. The samples were polished to a 600-grit finish, cleaned ultrasonically, and degreased with acetone prior to the test. Duplicate specimens were tested for each material/solution combination. The scan rate selected for these tests was 0.166 mV/s. All potentials were measured with respect to a Ag/AgCl reference electrode. After the tests, the samples were observed with an optical microscope for the presence of pits.

The molar anion concentrations of the thirteen simulated waste solutions which were used for the polarization scans are given in Table 1. The type of waste solution is also indicated in the table. These waste solutions, which were made from sodium salts, represent a range of concentrations which may be possible during the storage of the wastes. The tests were performed at 30 and 60° C, the anticipated temperature limits of the waste.

Coupon tests were conducted to confirm the cyclic polarization results. Metal coupons (2" x 1" x 0.125") were partially immersed in a simulated waste environment for three to four months. Four coupons were hung by teflon string in a polyethylene bottle filled with 500 ml of solution. Waterproof epoxy was applied to the coupon edge to prevent preferential attack. The temperature in the bottles was controlled with a water bath for tests at 30° C and with air circulating ovens for tests at 45° and 60° C. Air flow into the bottles was regulated at 100 cc/min to simulate the air flow in a waste tank.

Type 304L was tested in both the solution-annealed and the heat-treated conditions. The heat treatment was performed to simulate weld heat affected zones. The maximum degree of sensitization, as determined by electrochemical potentiokinetic reactivation (EPR), was obtained after heat treating the sample at 650° C for six hours. Welded coupons of 304L were also tested. The welds were single-pass gas tungsten arc welds. Comparison tests were performed on A537 carbon steel and Incoloy 825. A537, which is similar to the carbon steel used for the present waste tanks, is less corrosion resistant than 304L. The I825, a nickel based alloy, resists halide

attack and is more corrosion resistant than 304L. The compositions of each of the materials is shown in Table 3. The coupons were polished to a 600-grit finish and degreased with acetone prior to being immersed.

The 304L coupons were tested in waste solutions # 1, 4, 8, 11, and 13. These solutions were selected based on either a high concentration of chloride and fluoride or a lack of inhibitor species. The A537 and I825 coupons were tested in solutions # 1 and 8 only. The test matrix is shown in Table 2. After the coupons were removed, they were cleaned according to ASTM standard G 1-88. Optical light and scanning electron microscopy were used to evaluate the coupons for pit size, density and location.

EIS spectra were measured with a system that was controlled by an IBM PS/2 Model 30 personal computer with PAR Model 378 Electrochemical Impedance software. The sinusoidal waveform was generated by a PAR Model 5301A Lock-in Amplifier and applied to the sample through a PAR Model 273 Potentiostat/Galvanostat. The applied waveform had a 5 mV amplitude and a frequency range from 1 mHz to 100 kHz. The equilibrium state of the sample was characterized by measuring the open-circuit potential (E_{corr}) before and after each EIS test. The initial test was run after the sample was exposed for 2-3 days. The final test was performed after a three-month exposure, which was just prior to removal of the sample from the test.

Samples were prepared and exposed following a similar procedure described above for the coupon test, except that only 2 samples were placed in each bottle. An insulated, small-diameter, copper wire was spot welded to the top of the EIS coupons as a necessary electrical connection. The weld was covered with epoxy for protection. The EIS coupons included solution-annealed 304L and as-received A537. The waste environments were solution # 5 at 30°, 45° and 60° C. To perform an EIS test, a reference electrode and two graphite counter electrodes were inserted through the top of the bottle. The reference was a saturated calomel electrode (SCE) placed inside a salt bridge containing a saturated potassium chloride solution. The bottles were placed in a beaker of water heated to the appropriate temperature. At the conclusion of the test, a visual assessment of the corrosion was made for each sample.

Results and Discussion

All three tests demonstrated that 304L in the waste environments was not susceptible to localized corrosion. I825 also resisted attack in these environments, while A537 corroded in some cases. The results of each test are discussed in the following paragraphs.

Cyclic Polarization Tests

Cyclic polarization provides a quick assessment of a material's pitting susceptibility. In this study, pitting was determined from the hysterisis loop that developed when the current density for the reverse scan was greater than that of the forward scan. Previous work in waste solutions has demonstrated that this test is effective for predicting pitting attack, particularly if there was more than an order of magnitude difference in the current densities observed within the hysterisis loop[5].

The 304L specimens demonstrated no pitting susceptibility regardless of temperature, heat treatment or waste composition. Figure 1 shows the polarization curve for the test performed on solution-annealed 304L in solution #1 at 60° C. This curve is representative of all the tests that were conducted. No characteristic hysterisis loop or attack of the specimen surface was observed.

The I825 specimens were also not susceptible to pitting in any of the waste environments. Figure 2 is the polarization curve for the test performed in solution #1 at 60° C. Again, no hysterisis loop or specimen attack was observed for any of the waste solutions.

In contrast, the polarization tests indicated that A537 was susceptible to attack in several of the waste environments. The polarization curve shown in Figure 3 is from a test performed in solution #8 at 60° C. Severe crevice and uniform corrosion occurred on the specimen. The severity of attack was found to increase with temperature. The greatest overall attack occurred in the following wastes: the dilute wash waters (solutions # 2 and 5), the 30 % variation in the average cleaning solution concentration (solution # 8), and a decontamination cleaning solution (solution # 13). For these wastes, the inhibitor was insufficient to prevent attack by the aggressive anions.

E_{corr} values for each of the material/solution combinations are

shown in Table 4. For each material, the values ranged from -0.2 V for the dilute wash waters to -0.60 V for the unwashed slurry. E_{corr} appears to be dependent upon the concentration of the solution, but not on the material.

Coupon Tests

The results of the coupon tests were in good agreement with the results from the cyclic polarization tests. As expected, corrosion was not observed on either the 304L or I825 coupons in any of the tested solutions. The A537 coupons which were immersed in solution #1 were not corroded. The coupons which were in solution #8, however, were covered with isolated patches of corrosion products in the non-immersed areas of the coupons, at the water line, and in the crevice beneath the epoxy. The corrosion products displayed a tubular and flake morphology. The quantity of surface area covered by the corrosion products increased with solution temperature. After cleaning the sample, the area beneath the rust was examined and found to exhibit a shallow crater-like appearance reminiscent of uniform corrosion. The immersed areas of the coupons did not exhibit corrosive attack.

Although no pitting occured on the 304L samples in solutions #1, 4, 8, and 13, there was a thin precipitated layer on the immersed area and sporadic deposits on the non-immersed area. A precipitated layer was not found on samples which had been immersed in solution #11. The non-immersed area deposits observed for solutions #1, 4, 8, and 13 were white, coalesced crystals and were identified as gibbsite (Al_2O_3 $3H_2O$). The density of these deposits increased with the temperature and concentration of aluminate in the waste solution. The characteristics of the precipitates in the immersed area depended on the composition and temperature of the solution in which the coupon was immersed, but not on the material. The thickness of these layers was greatest near the waterline and tapered at greater depths beneath the interface. The initial surface marks on the immersed area in solutions #1, 4, and 8 were not obscured, while for solution #13 an approximately 1 mm thick film completely covered the marks. There was some variation in the morphology and composition of these precipitates. The precipitates from solutions #1 and 4 appeared as 3-4 micron size beads that were composed of aluminum, silicon, and sodium. As the temperature increased the density of the spheres increased while their size decreased. The precipitate from solution #8 had blue,

green or purple tints which gave the surface a luminescent appearance. The precipitates appeared as dry, cracked flakes that were approximately 10 microns across. They were composed of aluminum, sodium, phosporous and silicon. The solution #13 precipitate layer appeared as white, coalesced crystals which again were identified as gibbsite. At 30° C octahedral crystals were observed to be embedded in the gibbsite. These crystals were composed of aluminum, sodium and fluoride.

EIS

EIS was combined with the coupon test for a small number of samples to monitor for corrosion. The test results correlated well with the visual assessment of both the 304L and A537 samples. The results are summarized in Figures 4-9 as Bode plots of |Z| and the phase angle. The figures show the actual results for one of the samples at each temperature. Figures 4 and 5 are plots of |Z| and the phase angle for A537 at the start of the coupon test, respectively. Figures 6 and 7 are plots of |Z| and the phase angle for A537 at the finish of the coupon test, respectively. The final Bode plots of |Z| and the phase angle for 304L are shown in Figures 8 and 9, respectively.

The initial results for A537, shown in Figures 4 and 5, were similar to those for 304L. Both materials displayed a capacitive behavior which was independent of temperature. The capacitive behavior was characterized in the low frequency range (10 mHz-10 Hz). At frequencies less than 10 mHz, some A537 samples showed that |Z| leveled off with a corresponding decrease in the phase angle. These changes may indicate localized weakening of the passive oxide layer on A537.The high frequency range (>100 Hz) is dominated by the solution resistance.

The final EIS spectra as shown in Figures 8 and 9 for 304L were nearly identical to the initial spectra. The results were again independent of temperature. The lack of any change indicated that 304L maintained its passive oxide layer without any significant localized or general corrosion. E_{corr} for the samples changed over the course of the coupon test. Initial E_{corr} values ranged from -0.050 to +0.005 V (SCE) and final values ranged from +0.070 to +0.140 V (SCE).

Visual inspection of the samples revealed no corrosion, although a deposited surface layer was found on immersed sections of the samples. Such a layer may influence the EIS spectra. A more

rigorous deconvolution analysis of the results is being attempted. The EIS spectra, however, clearly showed that the samples were not corroding as was observed visually. The enoblement of E_{corr}, however, may be due to the formation of this surface layer. The surface layer had a fine granular structure at all temperatures and appeared the thickest on the samples exposed at 45° C. Small deposits were sporadically located on the part of the sample not immersed.

The final EIS spectra for A537 were significantly different from the initial spectra as shown by a comparison of Figures 4-7. Figures 6 and 7, which show the final Bode plots, were indicative of a corroding material. In the low frequency range (<10 Hz), final |Z| values were approximately an order of magnitude lower than the initial values and decreased with increasing temperature. The decrease in |Z| corresponded with a decrease in the maximum value of the phase angle and a shift in the maximum to higher frequencies. The change in the EIS spectra was accompanied by a change in E_{corr}. Initial values ranged from -0.025 to -0.20 V (SCE) and final values ranged from -0.180 to -0.240 V (SCE). A temperature dependence of E_{corr} was not observed. The visual assessment of the A537 samples revealed that corrosion was occurring. The non-immersed areas of the coupons were the most corroded. The corrosion products had a tubular and flake morphology. The size of the corroded area decreased with decreasing temperature. The immersed areas had a surface layer similar to that observed for 304L. The samples at all temperatures had some corroded spots on the immersed areas. Extensive corrosion was also observed beneath the epoxy. The shift in Ecorr to more active values was a result of this corrosion.

Correlation of Data with Actual Service

The results from the A537 coupon tests correlated well with observations of the present carbon steel tank walls. A tank that contained an uninhibited waste similar to solution #8, red, tubular, flake-like corrosion products were observed in the non-immersed area. After the tank walls were grit blasted to remove the corrosion products, shallow crater-like attack was seen at the water line and in the non-immersed area. The attack observed in the non-immersed and waterline areas may have occurred beneath deposits which were present in these areas. The immersed area, although it was covered with precipitated layers, did not corrode. This correlation between actual service and the laboratory tests allows one to place confidence

in these techniques as predictive tools. Therefore, based on the results of the laboratory tests, 304L will be a good selection for the materials of construction for the new waste tanks.

Conclusions

The cyclic polarization, coupon immersion and EIS tests demonstrated that 304L was not susceptible to attack in the simulated waste environments. I825 also did not corrode during any of the tests. In contrast, A537 showed susceptibility in some of the waste environments. The severity of the attack increased with temperature. The agreement between the laboratory tests for A537 and the corrosion which occured in actual service allows for confidence in these techniques as predictive tools. 304L was confirmed as a good choice for the materials of construction for the new waste tanks.

Acknowledgements

The authors thank P. E. Zapp, R. S. Ondrejcin and D. T. Hobbs of the Savannah River Laboratory for their comments. We also would like to recognize S. W. McCollum, C. N. Foreman, and A. P. Watkins for their assistance in conducting the experiments. The information contained in this article was developed under contract DE-AC09-89SR18035 with the U. S. Department of Energy.

References

1. J. R. Knight, "The Savannah River Plant and the Processing Facility Being Built to Prepare its Radioactive Waste for Permanent Disposal," Proc. AIChE Boston Meeting, American Institute of Chemical Engineers, New York, NY, 1986.
2. S. B. Oblath and J. W. Congdon, "Inhibiting Localized Corrosion During Storage of Dilute Wastes," Waste Management 87, Tuscon, AZ, 1987.
3. D. F. Bickford and C. M. Jantzen, Journal of Non-crystalline Solids, 84, (1986): p.299-307.
4. Z. Szklarska-Smialowska, Pitting Corrosion of Metals, (Houston, TX: National Association of Corrosion Engineers, 1986), p.201.
5. Private communication with P.E. Zapp

Table 1. Molar Anion Compositions of SimulatedWastes

Waste Solutions

Solution Number	1	2	3	4	5	6	7	8
pH	13.7	12.0	13.5	13.5	12.0	13.1	12.9	12.7
OH^-	2.1	0.03	1.1	1.3	0.024	0.66	0.21	0.15
$CO_3^=$	0.1	0.0015	0.051	0.16	0.0023	0.081	0.14	0.098
NO_2^-	1.1	0.016	0.56	0.6	0.0085	0.3	0.1	0.07
NO_3^-	1.4	0.02	0.71	2.0	0.028	1.0	0.54	0.7
Cl^-	0.022	0.00031	0.01	0.022	0.0004	0.011	0.001	0.0013
F^-	0.011	0.00016	0.0056	0.015	0.00022	0.0076	-	-
$SO_4^=$	0.095	0.0014	0.048	0.14	0.002	0.071	0.0061	0.0079
$Al(OH)_4^-$	0.3	0.0043	0.15	0.31	0.0045	0.16	0.01	0.007
$C_2O_4^=$	0.0051	0.000073	0.0026	0.014	0.0029	0.0085	-	-
$CrO_4^=$	0.0021	0.00003	0.0011	0.0033	0.000047	0.0017	0.0012	0.00084
$MoO_4^=$	0.00027	0.000004	0.00014	0.00043	0.000006	0.00022	-	-
$SiO_3^=$	0.0021	0.00003	0.0011	0.0038	0.000054	0.0019	0.00083	0.00058
PO_4^{-3}	0.0058	0.000084	0.0029	0.0085	0.00012	0.0043	0.02	0.014

1. Decanted solution from unwashed sludge slurry
2. Dilute wash water decanted from sludge slurry
3. 1:1 mixture of 1 and 2
4. Decontaminate supernate from salt slurry
5. Dilute wash water decanted from salt slurry
6. 1:1 mixture of 4 and 5
7. Average compositions of cleaning solution waste waste
8. 30 % variation of 7 for aggressive and passivating ions

Table 1. (cont.) Molar Anion Compositions of Simulated Wastes

	Waste Solutions				
Solution Number	9	10	11	12	13
pH	13.1	12.3	12.4	12.7	12.5
OH^-	0.361	0.01	-	0.01	-
NO_3^-	0.316	-	-	4.6	4.6
F^-	-	-	-	0.039	0.039
$Al(OH)_4^-$	-	-	-	0.26	0.26
$CrO_4^=$	-	0.013	0.013	-	-
PO_4^{-3}	-	0.22	0.22	-	-

9. Resin regeneration waste
10. Tritium target cleaning waste
11. Uninhibited tritium target cleaning waste
12. Cask decontamination waste
13. Unihibited cask decontamination waste

Table 2. Test Matrix for the Coupon Tests

Solution	1	4	5	8	11	13
Metal						
304L solution annealed	x	x		x	x	x
304L heat treate	x	x		x	x	x
304L welded	x	x		x	x	x
A 537 carbon steel	x			x		
Incoloy 825	x			x		
304L solution annealed impedance			xxx			
A 537 carbon steel impedance			xxx			

x- tests performed at 30, 45, and 60 C
xx- tests performed at 45 and 60 C
xxx- tests performed at 30, 45, and 60 C; two coupons per bottle

Table 3. Analysis of Materials Tested (wt. %)

	C	Mn	Si	P	S	Cr	Ni	Mo	Ti	Al	Fe	Cu
304L	.02	1.90	.85	.032	.02	19.4	8.9	--	--	--	bal.	--
A537	0.22	1.01	.032	.033	.031	.2	.21	.06	--		bal.	.22
I825	.02	.44	.23	--	.01	20.5	41.2	2.3	.85	.08	28.9	2.2

Table 4. E_{corr} (vs. Ag/AgCl) for the materials in the waste solutions at 60° C

Solution number	304L	304L heat treated	A537	I825
1	-0.373	-0.386	-0.410	-0.380
2	-0.217	-0.167	-0.232	-0.217
3	-0.297	-0.334	-0.390	-0.327
4	-0.368	-0.387	-0.455	-0.363
5	-0.223	-0.184	-0.278	-0.277
6	-0.354	-0.319	-0.380	-0.357
7	-0.302	-0.285	-0.352	-0.305
8	-0.31	-0.237	-0.268	-0.255
9	-0.315	-0.306	-0.318	-0.286
10	-0.33	-0.323	-0.412	-0.300
11	-0.338	-0.314	-0.387	-0.314
12	-0.292	-0.204	-0.307	-0.277
13	-0.325	-0.26	-0.238	-0.262

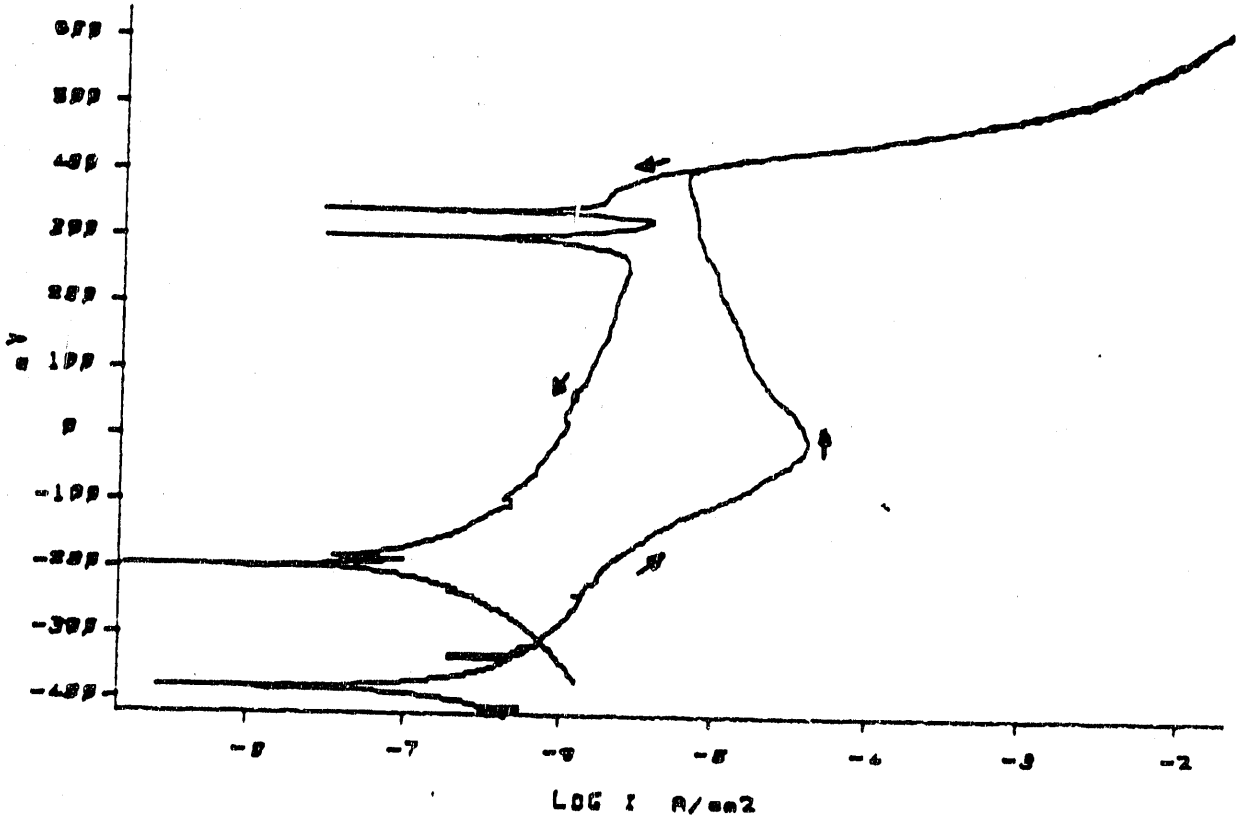

Figure 1. Polarization scan of 304L stainless steel in waste solution #1 at 60° C (vs. Ag/AgCl).

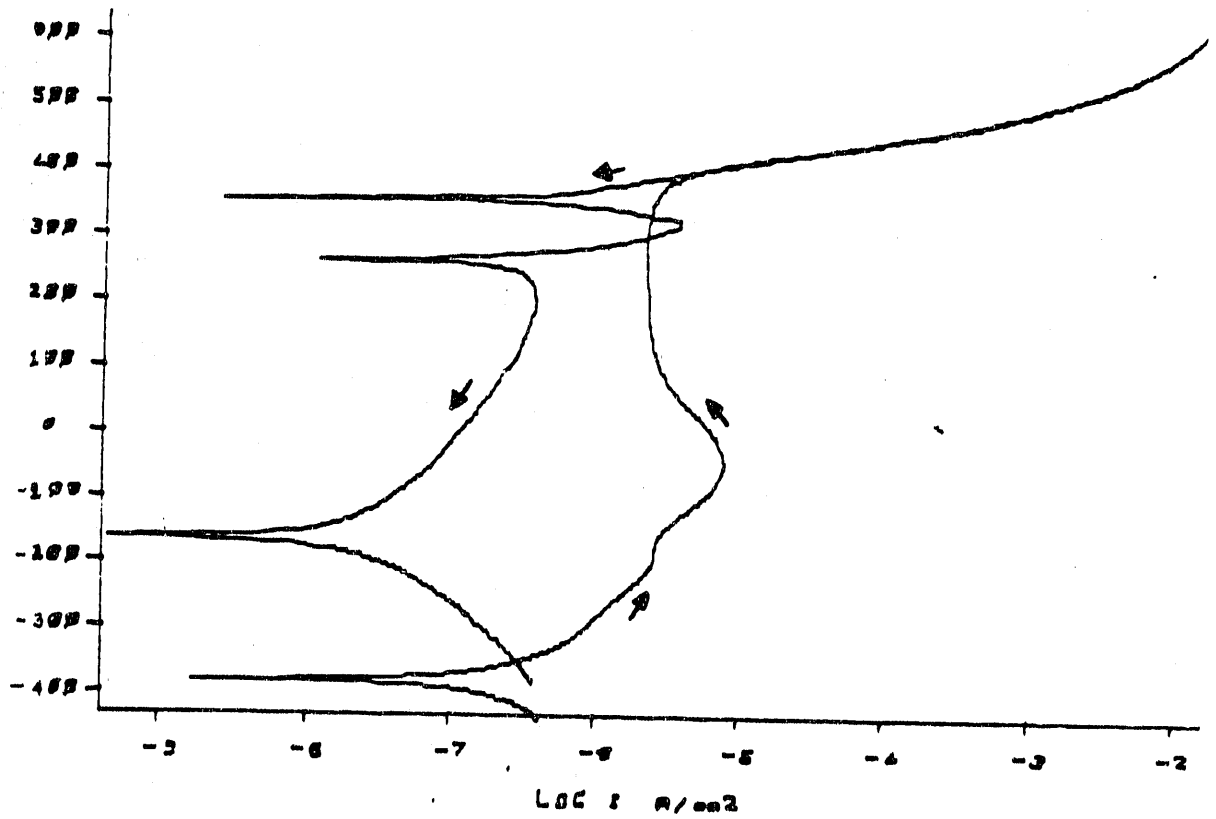

Figure 2. Polarization scan of I825 in waste solution #1 at 60° C (vs. Ag/AgCl).

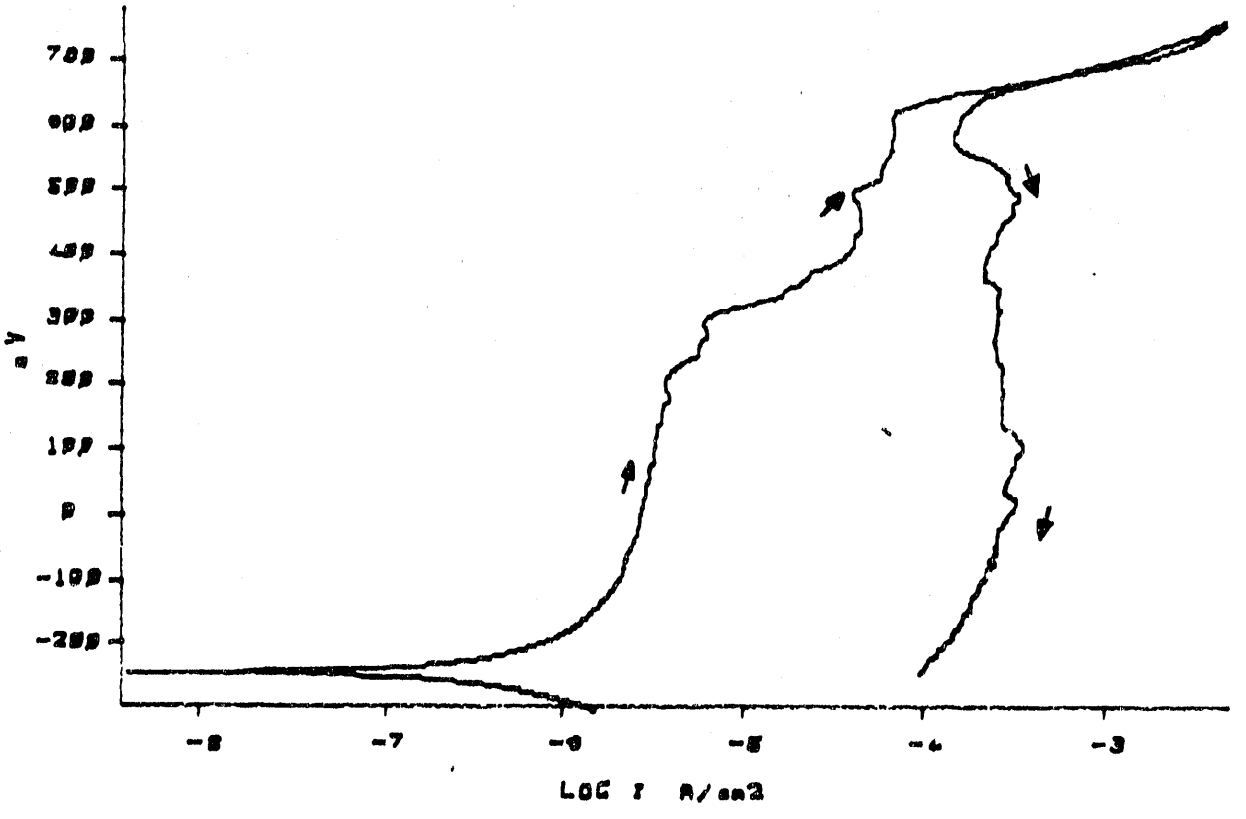

Figure 3. Polarization scan of A537 carbon steel in waste solution #1 at 60° C (vs. Ag/AgCl).

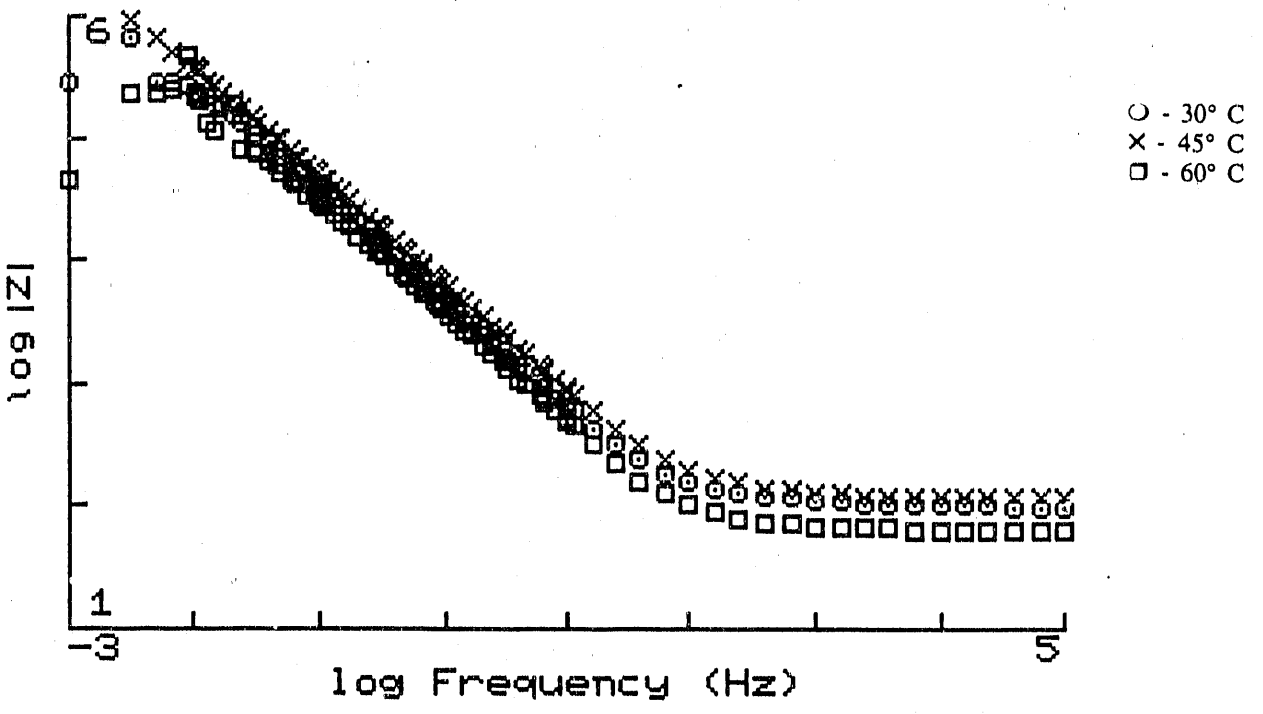

Figure 4. Initial Bode plot of $|Z|$ vs. the log frequency for A537 carbon steel at 30°, 45°, and 60° C.

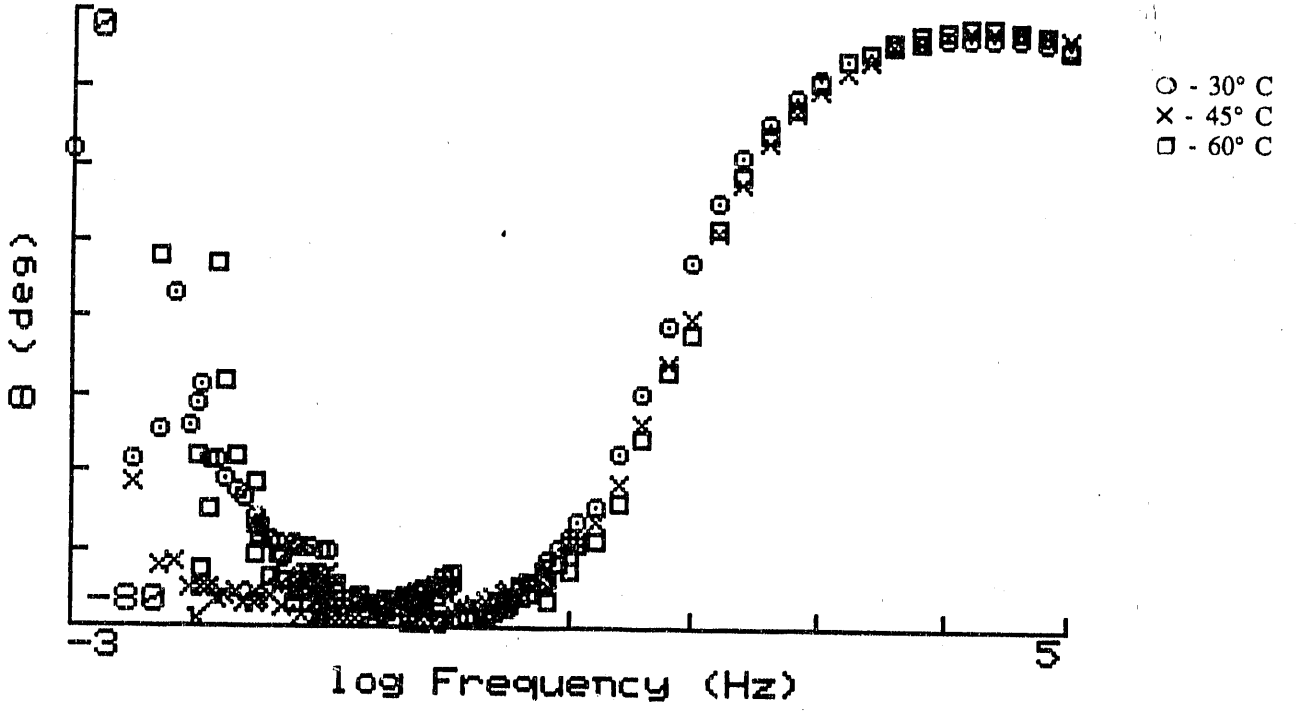

Figure 5. Initial Bode plot of the phase angle vs. the log frequency for A537 carbon steel at 30°, 45°, and 60° C.

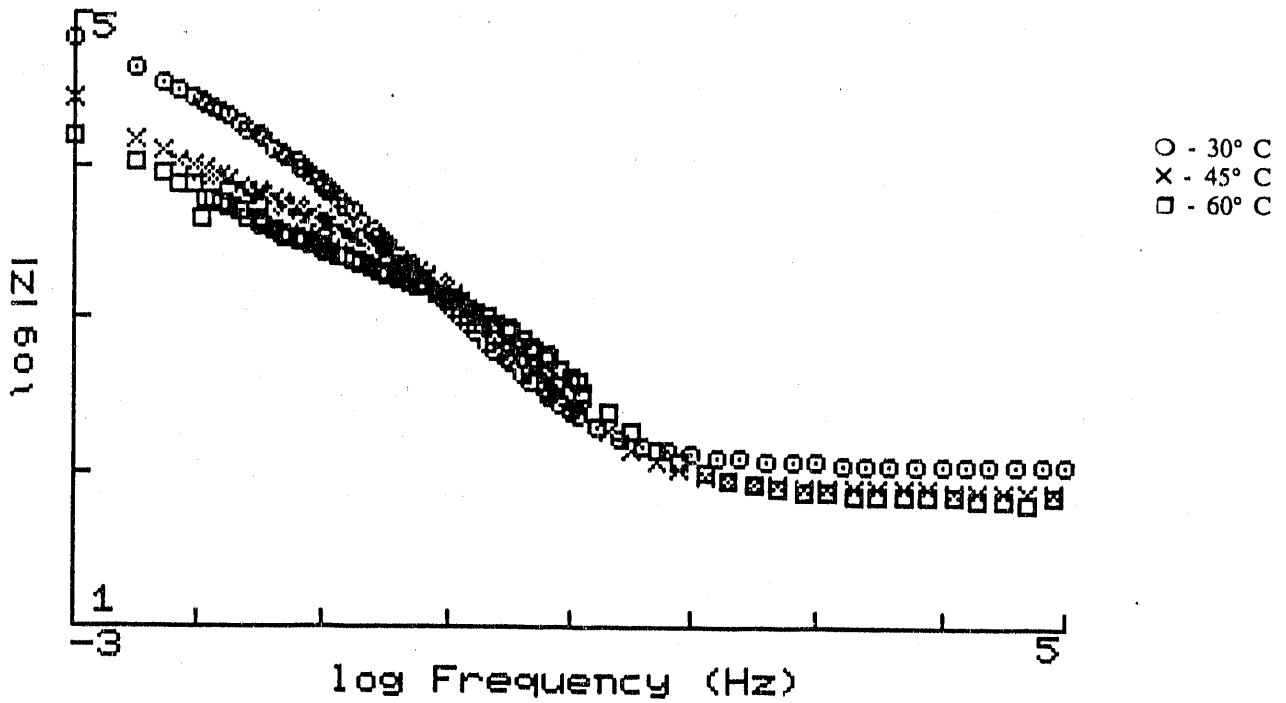

Figure 6. Final Bode plot of $|Z|$ vs. the log frequency for A537 carbon steel at 30°, 45°, and 60° C.

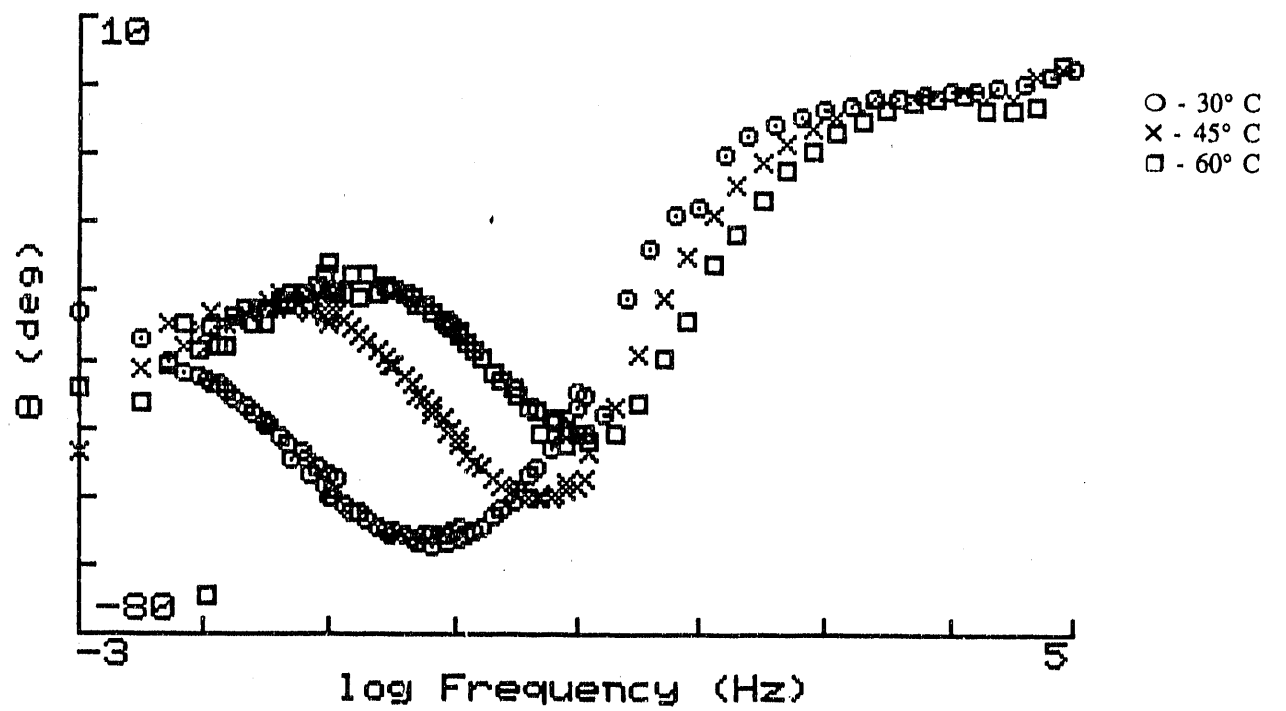

Figure 7. Final Bode plot of the phase angle vs. the log frequency for A537 carbon steel at 30°, 45°, and 60° C.

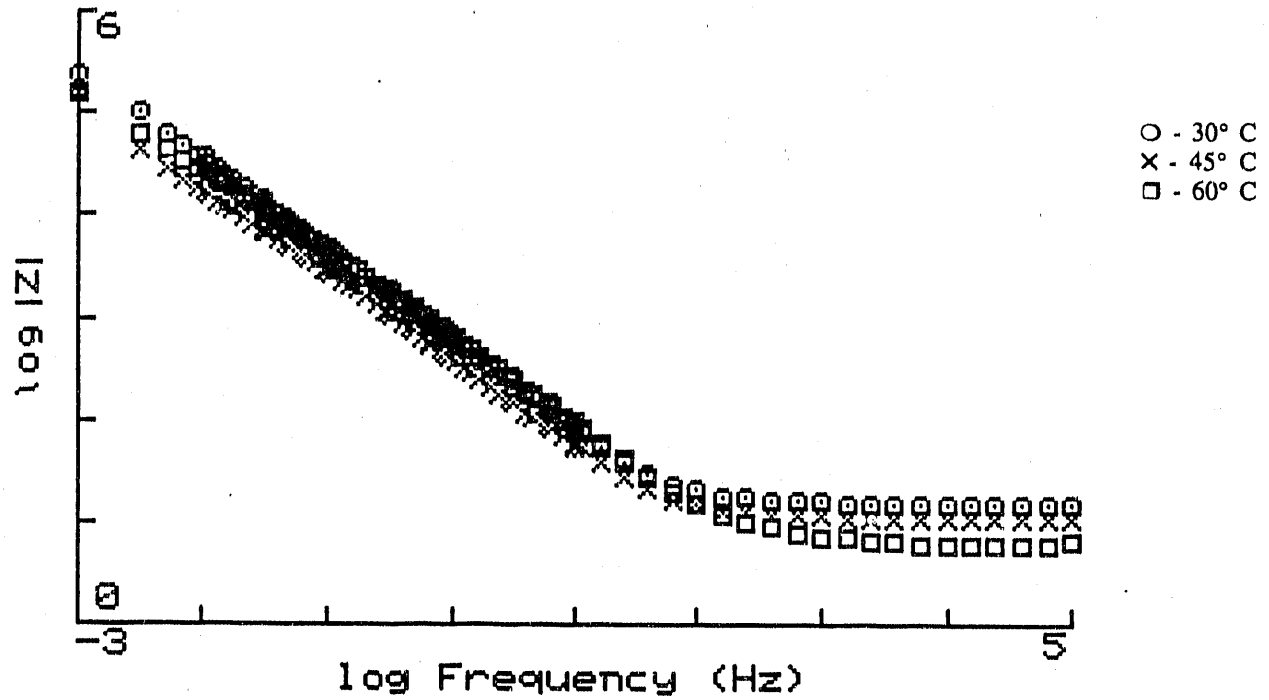

Figure 8. Final Bode plot of |Z| vs. the log frequency for 304L at 30°, 45°, and 60° C.

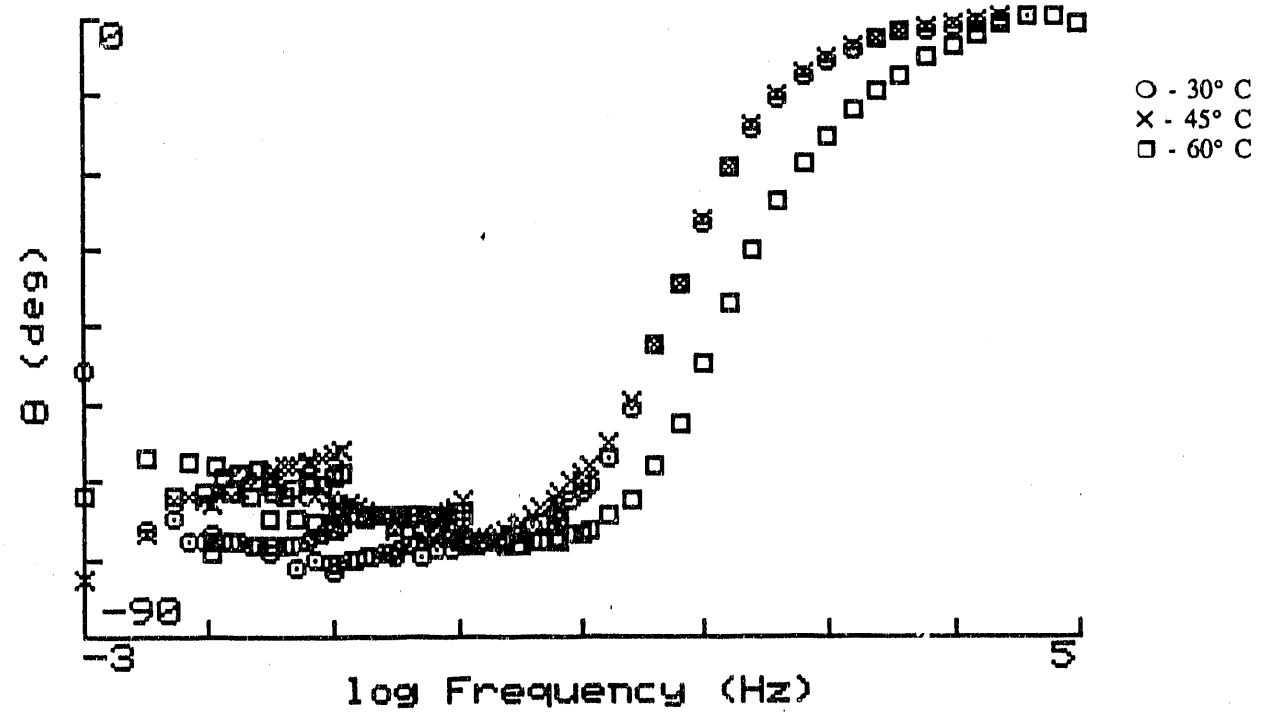

Figure 9. Final Bode plot of the phase angle vs. the log frequency for 304L at 30°, 45°, and 60° C.

DATE
FILMED
5/01/92